

# **Geophysical Research Letters**\*

# **RESEARCH LETTER**

10.1029/2022GL101041

#### **Key Points:**

- Van Allen Probes observed a simultaneous dropout of radiation belt electrons and ring current protons within 40 min accompanied by electromagnetic ion cyclotron (EMIC) waves
- The simulation indicates that fast EMIC wave scattering causes the dropout of electrons with energies
   1 MeV and pitch angles <75°</li>
- Concurrent dropout of protons with energies >200 keV and pitch angles >40° is also reproduced by EMIC wave scattering

#### Correspondence to:

X. Lyu, x10028@mix.wvu.edu

#### Citation:

Lyu, X., Ma, Q., Tu, W., Li, W., & Capannolo, L. (2022). Modeling the simultaneous dropout of energetic electrons and protons by EMIC wave scattering. *Geophysical Research Letters*, 49, e2022GL101041. https://doi.org/10.1029/2022GL101041

Received 27 AUG 2022 Accepted 14 OCT 2022

# **Modeling the Simultaneous Dropout of Energetic Electrons** and Protons by EMIC Wave Scattering

Xingzhi Lyu<sup>1</sup>, Qianli Ma<sup>2,3</sup>, Weichao Tu<sup>1</sup>, Wen Li<sup>3</sup>, and Luisa Capannolo<sup>3</sup>

<sup>1</sup>Department of Physics and Astronomy, West Virginia University, Morgantown, WV, USA, <sup>2</sup>Department of Atmospheric and Oceanic Sciences, University of California, Los Angeles, CA, USA, <sup>3</sup>Center for Space Physics, Boston University, Boston, MA, USA

**Abstract** Electromagnetic ion cyclotron (EMIC) waves could cause a simultaneous dropout of radiation belt electrons and ring current protons. However, their effects on the dropout of both plasma populations have not been quantified in previous studies. In this paper, we model the simultaneous dropout of MeV electrons and hundreds of keV protons observed by Van Allen Probes within  $\sim$ 40 min on 27 February 2014. The wave and particle measurements during the period of most intense EMIC waves at  $L \sim 5.2$  are used to calculate the quasilinear diffusion coefficients and simulate the evolution of both energetic electrons and protons. Our model well captures the dropout of electrons with energies >1 MeV and pitch angles <75°, and the concurrent dropout of protons with energies >200 keV and pitch angles >40°. This is the first modeling work quantitatively reproducing the simultaneous dropout of both populations due to EMIC wave scattering.

Plain Language Summary Electromagnetic ion cyclotron (EMIC) waves are one of the plasma waves in the Earth's magnetosphere. Both radiation belt electrons and ring current protons can be scattered by EMIC waves into the atmosphere within a short timescale (~hours). However, the role of EMIC waves in driving the simultaneous fast depletion of both populations has not been quantified. In this study, for the first time, we quantitatively modeled the temporal evolution of radiation belt electrons and ring current protons during a geomagnetic storm event based on the particle and wave observations by Van Allen Probes. The results suggest that EMIC wave scattering can efficiently cause the simultaneous depletion of both energetic electrons and protons on a timescale of ~40 min.

#### 1. Introduction

Recent observations by Van Allen probes have revealed the concurrent dropout of hundreds of keV ring current protons and MeV radiation belt electrons (Gkioulidou et al., 2016; Turner et al., 2014; Zhao et al., 2016). The fundamental question is where these energetic particles go during the dropout. Two main loss mechanisms have been identified in the previous studies for radiation belt electron dropouts (e.g., Morley et al., 2010; Shprits et al., 2016; Tu et al., 2014; Xiang et al., 2017), which include magnetopause shadowing (MPS) due to solar wind compression of the magnetopause combined with outward radial diffusion of electrons driven by Ultra-Low-Frequency (ULF) waves (e.g., Tu et al., 2019; Turner et al., 2012), and pitch angle scattering into the atmosphere by the interaction with electromagnetic ion cyclotron (EMIC) waves (e.g., Blum et al., 2015; Capannolo et al., 2019; Kersten et al., 2014; Usanova et al., 2014; Zhang et al., 2016). Theoretically, both mechanisms are also efficient in driving the fast loss of energetic protons at hundreds of keV to MeV energies in the ring current, which are usually co-located with the radiation belt electrons.

The latter mechanism known as EMIC wave scattering is the focus of this study and has been proved to be responsible for the fast loss of both energetic electrons and protons (Engebretson et al., 2018; Ni et al., 2022). For radiation belt electrons, Ma et al. (2015) used a 3-D diffusion code to simulate the evolution of energetic electron flux during a 10-day quiet period and found that EMIC waves are required to reproduce the decay of >1 MeV electron fluxes. Zhang et al. (2016) presented the direct and quantitative evidence of EMIC wave-driven relativistic electron loss in the Earth's radiation belts by comparing their model results and the local observations of pitch angle distributions during a dropout event. For the protons, Jordanova et al. (2001, 2008) modeled the ring current proton precipitation by including EMIC waves during geomagnetic storm periods and their results generally show good agreement with the observations. Usanova et al. (2010) analyzed the EMIC wave excitation during a storm event using the ground and multi-satellite measurements and the results indicated that EMIC waves efficiently

© 2022. American Geophysical Union. All Rights Reserved.

LYU ET AL.

accounted for the localized precipitation of protons with energies >30 keV. During the dropout events, the particle fluxes decrease and the EMIC waves may occur within a short timescale. Whether the same EMIC wave burst could be the dominant contributor to the simultaneous fast loss of both electrons and protons remains a question.

A few comparative studies have revealed the concurrent precipitation between the radiation belt electrons and ring current protons (Carson et al., 2012; Engebretson et al., 2015). Miyoshi et al. (2008) showed the coincident precipitation of tens of keV ions and relativistic electrons on 5 September 2005 based on the unique set of ground and satellite measurement. Usanova et al. (2014) reported simultaneous 30–800 keV proton precipitation and narrowing of multi-MeV electron pitch angle distributions toward 90° due to the interaction with EMIC waves during a moderate geomagnetic storm on 11 October 2012. Since the previous works discussed above are either qualitative or only focus on one particle population, a comprehensive comparative study is needed to quantitatively understand the role of EMIC wave scattering in the simultaneous dropout of energetic electrons and protons. In this paper, for the first time, we model the fast particle loss due to EMIC wave scattering using the Van Allen Probes observations during the geomagnetic storm in February 2014, to quantify the role of EMIC wave scattering in the simultaneous dropout of radiation belt electrons and ring current protons.

# 2. Event Analysis

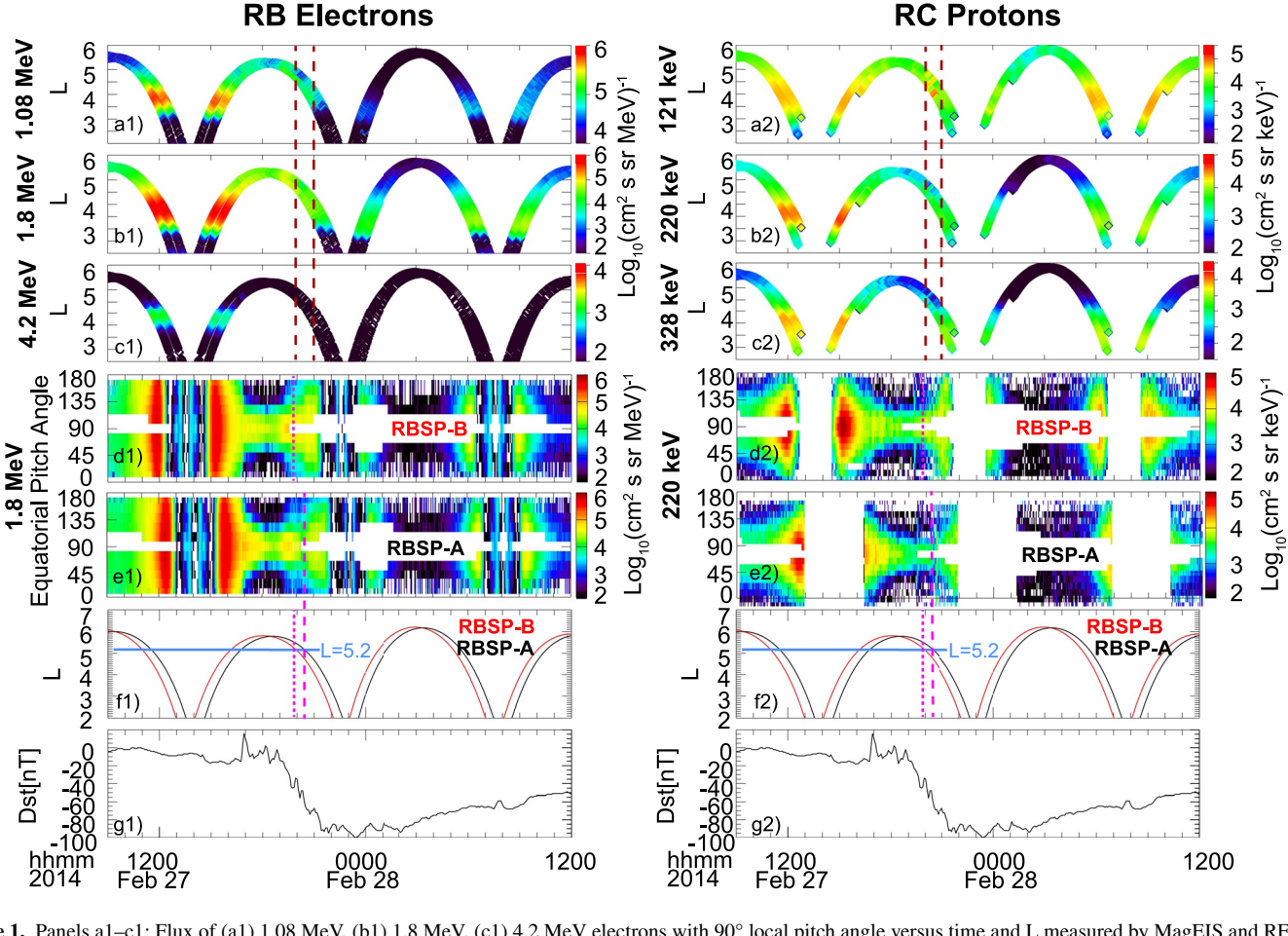
Van Allen Probes provide detailed in situ measurements of both particles and plasma waves in the Earth's inner magnetosphere (Mauk et al., 2013). Electron fluxes measured by the Magnetic Electron Ion Spectrometer (MagEIS) (Blake et al., 2013) and Relativistic Electron Proton Telescope (REPT) instruments (Baker et al., 2013) are used in this study. The MagEIS instrument measures electrons over the energy range of ~30 keV to ~4 MeV, while the REPT instrument measures highly energetic electrons with an energy range of ~1.5–20 MeV. Energetic proton fluxes used in the present work are from the measurements of the Radiation Belt Storm Probes Ion Composition Experiment (RBSPICE) instrument (Mitchell et al., 2013) with an energy range of 10–600 keV. In addition, the Electric and Magnetic Field Instrument Suite and Integrated Science (EMFISIS) instrument with high time resolution (64 sample/s) triaxial fluxgate magnetometers (Kletzing et al., 2013) provides the EMIC wave measurements in our analysis.

Figure 1 presents an overview of the energetic electron (left column) and proton (right column) flux evolution from 09 UT on February 27 to 12 UT on 28 February 2014. Figures 1a1-1c1 show the electron fluxes at different energies of 1.08, 1.8, and 4.2 MeV as a function of time and dipole L shell, measured by MagEIS and REPT instruments onboard Van Allen Probes. 121, 220, and 328 keV proton fluxes measured by the RBSPICE instrument are plotted in the same way, as shown in Figures 1a2-1c2. The Dst index is shown in Figures 1g1 and 1g2, which indicates the storm commencement at  $\sim 18:00$  UT on February 27. The observed fluxes for MeV electrons and 100s keV protons exhibited simultaneous dropout outside L=3.3 during the inbound of both probes at the end of February 27. The equatorial pitch angle distributions of 1.8 MeV electrons and 220 keV protons measured by two probes are shown in Figures 1d1, 1e1, 1d2, and 1e2, respectively, with the equatorial pitch angles calculated from local pitch angles using the TS04 magnetic field model (Tsyganenko & Sitnov, 2005). The flux measurements of electrons and protons generally have a good coverage over all equatorial pitch angles, except for some data gaps close to  $90^{\circ}$  during the storm main phase.

The two red dashed lines in the top three panels on both sides of Figure 1 mark the 1-hr period when EMIC waves are observed (Figure 2). Figure 2a shows the magnetic field power spectral density and Figure 2b shows the integrated EMIC wave amplitude for hydrogen-band (H-band) and helium-band (He-band) measured by Van Allen Probe A during 20:00–21:00 UT on 27 February 2014. The information of latitude, L\* from the TS04 model, L, and MLT along the orbit is shown at the bottom of Figure 2b. For the 1-hr EMIC wave observations, the MLT spans from 13.0 to 13.9 and the L shell changes from 5.4 to 4.6. The EMIC waves are shown to have strong wave power in the He-band frequencies and moderate wave power in the H-band at higher L during ~20:10-20:30 UT, followed by intense wave power in both H-band and He-band frequencies during ~20:40–21:00 UT. To quantify the effect of EMIC wave scattering, we selected the most intense wave activities located at  $L \sim 5.2$ , as denoted by the two dashed vertical magenta lines in Figures 2a and 2b. Then to analyze the evolution of both electrons and protons before and after the observed waves, we obtained the electron and proton measurements by two probes when they traveled to the same L shell as the EMIC waves (at L = 5.2 as illustrated by the blue horizontal lines in Figures 1f1 and 1f2), first by Probe B as marked by the dotted lines in Figures 1d1 and 1d2, then by Probe A at 40 min later marked by the dashed lines in Figures 1e1 and 1e2. The detailed phase space density (PSD)

LYU ET AL. 2 of 8

19448007, 2022, 20, Downloaded from https://agupubs.onlinelibrary.wiley.com/doi/10.1029/2022GL101041 by West Virginia University, Wiley Online Library on [21/12/2022]. See the Terms and Conditions (https://onlin



**Figure 1.** Panels a1–c1: Flux of (a1) 1.08 MeV, (b1) 1.8 MeV, (c1) 4.2 MeV electrons with 90° local pitch angle versus time and L measured by MagEIS and REPT instruments onboard Van Allen Probes (RBSP) from 02-27/09 UT to 02-28/12 UT in 2014. Panels a2–c2: Flux of (a2) 121 keV, (b2) 220 keV, (c2) 328 keV protons with 90° local pitch angle versus L and time measured by RBSPICE instrument during the same time period as of electrons. Panels d1, e1, d2, and e2: Evolution of equatorial pitch angle distributions of 1.8 MeV electrons (left) and 220 keV protons (right) measured by Van Allen Probe B (d1 and d2) and A (e1 and e2). Panels f1 and f2: L shells of Van Allen Probe B (red) and A (black). Panels g1 and g2: Dst index. The two dark red dashed lines in panels a1–c1 and a2–c2 correspond to the period marked in Figures 2a and 2b when electromagnetic ion cyclotron (EMIC) waves were observed. The magenta dotted lines in panels d1, d2, f1, and f2 indicate the time before EMIC waves were observed when the equatorial pitch angle distributions of electrons (left) and protons (right) observed by Probe B at L = 5.2 were used in the modeling, while the dashed lines represent the time after EMIC waves were observed when Probe A traveled to the same L.

evolutions of electrons and protons are shown in Figures 3a and 3e. Each panel shows the observed PSD versus equatorial pitch angle profiles with different colors representing different energies of particles. The dotted curves are the measurements made by probe B at  $L \sim 5.2$  at  $\sim 19:50$  UT, which is before the EMIC wave observation and taken as the initial condition of our simulation which will be described in the next section. The dashed curves show the distributions observed by Probe A, which is 40 min later when it crossed the same L shell and observed strong EMIC waves. Figure 3a shows that the electron PSD drops over a wide range of equatorial pitch angles with more significant losses at higher energies. Figure 3e shows that the concurrent proton PSD dropout only occurs at high equatorial pitch angles especially at energies above 200 keV, while at energies of 182-331 keV the proton PSD are observed to increase at lower pitch angles below  $\sim 75^{\circ}$ .

## 3. Simulation Results

To simulate the PSD evolution of both populations, we performed a 2-D pitch angle and energy diffusion simulation by solving the Fokker-Planck equation (Ma et al., 2012). Diffusion coefficients driven by the observed H-band and He-band EMIC waves at  $L \sim 5.2$  (shown between the two vertical magenta dashed lines in Figure 2a) for both electrons and protons are calculated using the Full Diffusion Code (Ma et al., 2019). We use the observed EMIC wave frequency spectrum averaged during 20:16–20:20 UT. The total electron density is 180 cm<sup>-3</sup>, and

LYU ET AL. 3 of 8

19448007, 2022, 20, Downloaded from https://agupubs.onlinelibrary.wiley.com/doi/10.1029/2022GL101041 by West Virginia University, Wiley Online Library on [21/12/2022]. See the Terms and Conditions (https://onlinelibrary.v

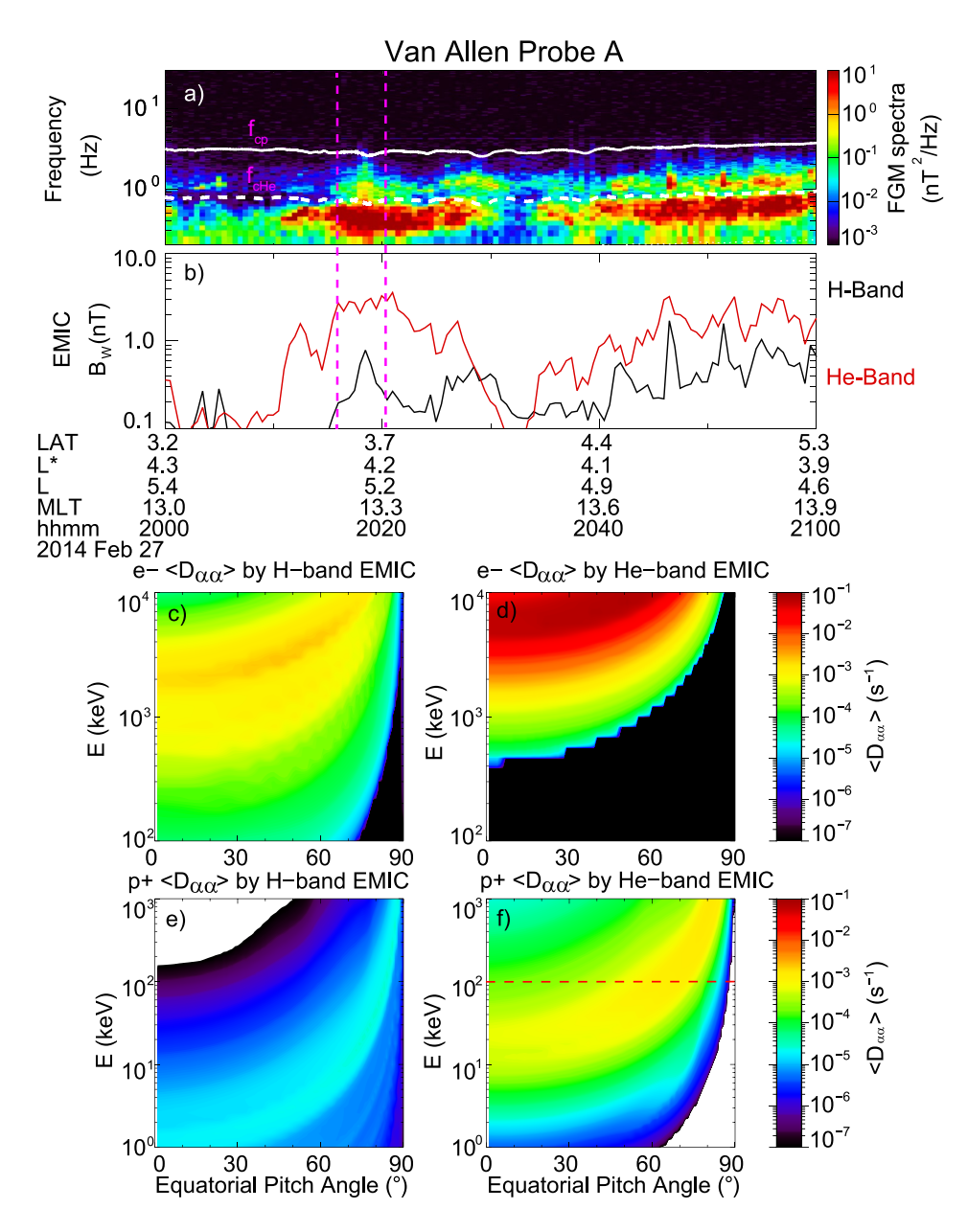


Figure 2. Electromagnetic ion cyclotron (EMIC) wave observations during 20:00–21:00 UT on February 27 by Van Allen Probe A. (a) EMIC wave magnetic field spectral density. (b) The integrated EMIC wave amplitudes for Hydrogen-band (H-band, black) and Helium-band (He-band, red). (c–f): Bounce-averaged pitch angle ( $<D_{cac}>$ ) diffusion coefficients of electrons (panels c and d) and protons (panels e and f) for each band of EMIC waves, with the hydrogen band on the left and the helium band on the right. The white lines in panel (a) denote the equatorial proton and helium gyrofrequencies. The two dashed vertical magenta lines in panels (a and b) indicate the period of waves used for the calculation of diffusion coefficients shown in panels (c–f). The region above the horizontal red dashed line in panel (f) marks the energies focused on (>100 keV protons) in this study.

the proton gyrofrequency at the equator is 2.8 Hz. The resonance number in the calculation spans from -5 to 5 including the Landau resonance. The observed intense EMIC waves were assumed to have 2 hr coverage in MLT for both H-band ( $\sim$ 0.5 nT) and He-band ( $\sim$ 1.5 nT) waves. The cold ion composition was assumed to be 90% H<sup>+</sup>, 5% He<sup>+</sup> and 5% O<sup>+</sup>. We used the latitudinally varying wave normal angle distribution from Ni et al. (2015), which changes from field-aligned at the equator to more oblique at higher latitudes up to 40°. The waves were also assumed to be located below the latitudes where the wave frequencies are equal to the crossover frequency.

LYU ET AL. 4 of 8

19448007, 2022, 20, Downloaded from https://agupubs.onlinelibrary.wiley.com/doi/10.1029/2022GL101041 by West Virginia University, Wiley Online Library on [21/12/2022]. See

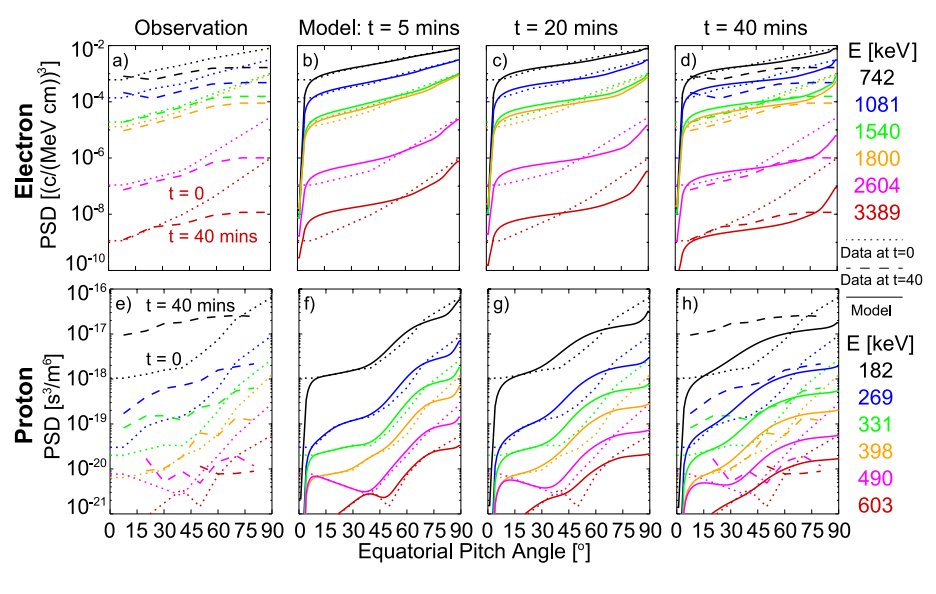


Figure 3. Panels (a and e): Observed (a) electron and (e) proton pitch angle distributions by Van Allen Probes at L = 5.2 at t = 0 and 40 min. Solid lines in panels (b–d and f–h): Modeled Evolution of electron (b–d) and proton (f–h) pitch angle distributions due to the interaction with electromagnetic ion cyclotron waves at the simulation times of t = 5, 20, 40 min, respectively. Initial distributions at t = 0 are shown as dotted curves in all the panels, and final observations at t = 40 min are plotted as dashed curves in panels (d and h).

The calculated bounce-averaged pitch angle diffusion coefficients  $< D_{\alpha\alpha} >$  due to different bands of EMIC waves for both electrons and protons are shown in Figures 2c-2f. The  $< D_{\alpha\alpha} >$  are plotted as a function of equatorial pitch angle and energy. The He-band EMIC wave diffusion rates for electrons and protons are shown to be higher than the H-band diffusion rates due to the higher wave intensity observed in the He-band than the H-band (Figure 2a). Although EMIC wave power close to the ion gyrofrequencies was observed, the peak wave power was at lower frequencies; therefore, Figure 2d shows that the rapid pitch angle diffusion of electrons is confined to MeV energies with a timescale shorter than a few minutes, which is consistent with previous studies (e.g., Li et al., 2007; Usanova et al., 2014; Zhang et al., 2016). At energies below  $\sim$ 5 MeV, the diffusion rates of electrons are larger at lower equatorial pitch angles and smaller at equatorial pitch angles closer to  $90^{\circ}$ . It means faster loss at lower pitch angles, and a  $90^{\circ}$ -peaked pitch angle distribution would be formed. On the other hand, Figure 2f shows that the He-band  $< D_{\alpha\alpha} >$  of protons at low pitch angles is peaked at tens of keV energy. Since the proton dropout was mainly observed at hundreds of keV during this event, we focus on the diffusion coefficients above 100 keV (marked by the red dashed line in Figure 2f). The  $< D_{\alpha\alpha} >$  is found to be highest at  $60-80^{\circ}$  equatorial pitch angles at 0.1-1 MeV energies, and the pitch angle of peak  $< D_{\alpha\alpha} >$  is higher at higher energies.

The drift periods of MeV electrons and hundreds of keV protons at L = 5.2 are on the timescale of a few minutes and tens of minutes, respectively. To perform a 40-min Fokker Planck simulation, we considered the MLT coverage of EMIC waves and scaled the diffusion rates accordingly. For the boundaries of the simulation, we used zero-gradient boundary conditions at pitch angles of 0° and 90° for the pitch angle operator, and the observed PSDs at lower energy (100 keV) and upper energy (electron: 10 MeV; proton: 1 MeV) boundaries. The initial conditions used in the model are the pitch angle distribution of the PSD data measured by Van Allen Probe B for electrons and protons, shown as the dotted curves in Figure 3. Figures 3b-3d present the simulated electron PSD at times of t = 5, 20, and 40 min respectively of the model run denoted by the solid curves. The dashed curves in Figures 3d and 3h correspond to the final observed PSD distributions at t = 40 min. For electrons, we find that the simulated PSD evolutions show faster losses at higher energies and 90° peaked pitch angle distributions after the losses. Comparing the modeled PSD and observations at t = 40 min (solid and dashed curves in Figure 3d), we can see our model well reproduced the dropout features of electrons at energies >1 MeV and equatorial pitch angle <75°. We also noticed that the model underestimated the PSD loss of 742 and 1,081 keV electrons. Therefore, we checked the whistler-mode wave observations and found that the plasmaspheric hiss were observed simultaneously (not shown) with the EMIC waves, which could potentially drive the additional loss of lower energy (742 and 1,081 keV) electrons. The hiss waves could also reduce the electron PSD at  $\sim$ 90° pitch angle and

LYU ET AL. 5 of 8



form a more flattened pitch angle distribution at several MeV energies (Ma et al., 2015). Figures 3f-3h show the modeled PSD evolution of 100s keV protons at the same times as the electrons. The loss of the simulated proton PSD is faster at higher pitch angles and the pitch angle anisotropy is gradually reduced from the initial condition at each energy. The comparison between the model results and observations at t = 40 min show good agreement at proton energies >200 keV and pitch angles >40° in terms of both the PSD level and the pitch angle distribution shape. At 182 keV energy, the observation shows a large PSD enhancement at pitch angles <75°, which is underestimated by the simulation. This could be due to some additional source (such as injection) of <200 keV protons during the storm main phase that is not included in the model. However, our simulation suggests that the evolution of higher energy protons (>200 keV) is mainly caused by resonant interaction with EMIC waves during the 40-min interval.

#### 4. Conclusions and Discussions

Using high-resolution particle and wave measurements from Van Allen Probes, we reported the simultaneous dropout of MeV radiation belt electrons and 100s keV ring current protons observed on 27 February 2014, and then analyzed the relevance of the dropout with the observed EMIC waves (only H-band and He-band EMIC waves were detected). Taking advantage of the dual-probe observations during this event, we investigated the energy and pitch angle dependence of the local losses of both energetic electrons and protons at  $L \sim 5.2$ , where the most intense EMIC waves were observed. The Van Allen Probe B was ~40 min ahead of Probe A when traveling through  $L \sim 5.2$  along the inbound orbit. Comparing the equatorial pitch angle distributions measured by the two probes, we found that the fast dropout of electrons happened mainly at small to intermediate equatorial pitch angles (<75°) and MeV energies, and the dropout of protons occurred mainly at high pitch angles (closer to 90°) and several hundred keV energies. The signatures of electron flux dropout are consistent with the loss features induced by EMIC waves as predicted by previous modeling studies (e.g., Li et al., 2007; Zhang et al., 2016).

To quantify the effects of EMIC wave scattering in the observed simultaneous dropouts of energetic electrons and protons, we implemented a 2-D pitch angle and energy diffusion model based on the quasilinear theory to simulate the PSD evolution of both populations caused by the observed waves. First, event-specific diffusion coefficients for electrons and protons are calculated using the observed H-band and He-band EMIC wave power spectra by Van Allen Probe A. The diffusion rates due to He-band EMIC waves are found to be higher than the diffusion rates due to H-band EMIC waves. The bounce-averaged diffusion coefficients  $< D_{\alpha\alpha} >$  driven by He-band EMIC waves show that the electron diffusion rate is larger at lower equatorial pitch angles and higher energies up to  $\sim$ 5 MeV. The diffusion rates of protons at energies higher than 100 keV are shown to be larger at intermediate pitch angles (e.g.,  $\sim$ 60°–75° for 200 keV protons) and smaller on both the low and high ends of the pitch angle range. These theoretical features match the particle observations mentioned above.

Using the equatorial pitch angle distributions of particles measured by Van Allen Probe B as the initial conditions and setting up proper boundary conditions, we performed the simulation for the dropout of both radiation belt electrons and ring current protons. The detailed simulation results show that the model well reproduces the dropout of electrons with energies of >1 MeV and equatorial pitch angles <75°. Hiss wave scattering may contribute to the additional loss of electrons at energies below ~1 MeV and pitch angles close to 90°. The concurrent dropout of protons with energies >200 keV and equatorial pitch angle >40° are also well explained by the EMIC wave scattering. The underestimation of the 182 keV proton PSD is possibly due to some additional source (like injection) during the storm main phase. The magnetopause shadowing may have a weaker effect on the particle loss than EMIC wave scattering at  $L \sim 5.2$  during this event, because the last closed drift shell was at higher L shell values than the Van Allen Probes' orbit (Xiang et al., 2017). We have also investigated observations from the low-altitude NOAA POES satellites (Evans & Greer, 2004) during the dropout (not shown), which show clear and strong tens to hundreds of keV proton precipitation at similar L and MLT region as the dropout observed by Van Allen Probes, lasting from ~19:00 to ~22:00 UT. Electron precipitation at >700 keV was observed in this region at ~19:29 UT and POES revealed that the trapped >700 keV electron population was present (high electron flux) until ~19:30 UT and was progressively depleted, in agreement with the electron dropout observed by Van Allen Probes. In summary, to the best of our knowledge, this study is the first quantitative simulation demonstrating the important role of EMIC wave scattering in the simultaneous dropout of both radiation belt electrons and ring current protons.

LYU ET AL. 6 of 8

19448007, 2022, 20, Downloa

Wiley Online Library on [21/12/2022]. See

# **Data Availability Statement**

The model inputs and outputs in this paper are publicly available from the data repository https://doi.org/10.5281/zenodo.7026538.

#### Acknowledgments

This work was supported by NASA Grants 80NSSC21K1312 and 80NSSC21K2008, NSF Grant AGS 1752736, and Cottrell Scholar Award ID 25883. OM would like to acknowledge the NASA Grant 80NSSC20K0196. WL would like to acknowledge NASA Grants 80NSSC20K1270 and 80NSSC20K0698, NSF Grant AGS-2019950, and Alfred P. Sloan Research Fellowship FG-2018-10936. We acknowledge the Van Allen Probes data from MagEIS and REPT instrument obtained from https:// rbsp-ect.newmexicoconsortium.org/ science/DataDirectories.php, data from RBSPICE instrument obtained from http://rbspice.ftecs.com/Data.html, and data from EFMISIS instrument obtained from https://emfisis.physics.uiowa.edu/

### References

- Baker, D. N., Kanekal, S. G., Hoxie, V. C., Batiste, S., Bolton, M., Li, X., et al. (2013). The Relativistic Electron-Proton Telescope (REPT) instrument on board the Radiation Belt Storm Probes (RBSP) spacecraft: Characterization of Earth's radiation belt high-energy particle populations. Space Science Reviews, 179(1–4), 337–381. https://doi.org/10.1007/s11214-012-9950-9
- Blake, J. B., Carranza, P. A., Claudepierre, S. G., Clemmons, J. H., Crain, W. R., Dotan, Y., et al. (2013). The Magnetic Electron Ion Spectrometer (MagEIS) instruments aboard the Radiation Belt Storm Probes (RBSP) spacecraft. Space Science Reviews, 179(1–4), 383–421. https://doi.org/10.1007/s11214-013-9991-8
- Blum, L. W., Halford, A., Millan, R., Bonnell, J. W., Goldstein, J., Usanova, M., et al. (2015). Observations of coincident EMIC wave activity and duskside energetic electron precipitation on 18–19 January 2013. Geophysical Research Letters, 42(14), 5727–5735. https://doi.org/10.1002/2015GL065245
- Capannolo, L., Li, W., Ma, Q., Shen, X.-C., Zhang, X.-J., Redmon, R. J., et al. (2019). Energetic electron precipitation: Multievent analysis of its spatial extent during EMIC wave activity. *Journal of Geophysical Research: Space Physics*, 124(4), 2466–2483. https://doi.org/10.1029/2018IA026291
- Carson, B. R., Rodger, C. J., & Clilverd, M. A. (2012). POES satellite observations of EMIC-wave driven relativistic electron precipitation during 1998–2010. *Journal of Geophysical Research*, 118(1), 232–243. https://doi.org/10.1029/2012JA017998
- Engebretson, M. J., Posch, J. L., Braun, D. J., Li, W., Ma, Q., Kellerman, A. C., et al. (2018). EMIC wave events during the four GEM QARBM challenge intervals. *Journal of Geophysical Research: Space Physics*, 123(8), 6394–6423. https://doi.org/10.1029/2018JA025505
- Engebretson, M. J., Posch, J. L., Wygant, J. R., Kletzing, C. A., Lessard, M. R., Huang, C., et al. (2015). Van Allen probes, NOAA, GOES, and ground observations of an intense EMIC wave event extending over 12 h in magnetic local time. *Journal of Geophysical Research: Space Physics*, 120(7), 5465–5488. https://doi.org/10.1002/2015JA021227
- Evans, D. S., & Greer, M. S. (2004). Polar orbiting environmental satellite space environment monitor-2: Instrument descriptions and archive data documentation archive data documentation. NOAA Technical Memorandum 93, Version 1.4. Space Weather Prediction Center.
- Gkioulidou, M., Ukhorskiy, A. Y., Mitchell, D. G., & Lanzerotti, L. J. (2016). Storm time dynamics of ring current protons: Implications for the long-term energy budget in the inner magnetosphere. Geophysical Research Letters, 43(10), 4736–4744. https://doi.org/10.1002/2016GL068013
- Jordanova, V. K., Albert, J., & Miyoshi, Y. (2008). Relativistic electron precipitation by EMIC waves from self-consistent global simulations. Journal of Geophysical Research, 113(A3), A00A10. https://doi.org/10.1029/2008JA013239
- Jordanova, V. K., Farrugia, C. J., Thorne, R. M., Khazanov, G. V., Reeves, G. D., & Thomsen, M. F. (2001). Modeling ring current proton precipitation by electromagnetic ion cyclotron waves during the May 14–16, 1997, storm. *Journal of Geophysical Research*, 106(A1), 7–22. https://doi.org/10.1029/2000JA002008
- Kersten, T., Horne, R. B., Glauert, S. A., Meredith, N. P., Fraser, B. J., & Grew, R. S. (2014). Electron losses from the radiation belts caused by EMIC waves. *Journal of Geophysical Research: Space Physics*, 119(11), 8820–8837. https://doi.org/10.1002/2014JA020366
- Kletzing, C. A., Kurth, W. S., Acuna, M., MacDowall, R. J., Torbert, R. B., Averkamp, T., et al. (2013). The electric and magnetic field instrument suite and integrated science (EMFISIS) on RBSP. Space Science Reviews, 179(1–4), 127–181. https://doi.org/10.1007/s11214-013-9993-6
- Li, W., Shprits, Y. Y., & Thorne, R. M. (2007). Dynamic evolution of energetic outer zone electrons due to wave-particle interactions during storms. *Journal of Geophysical Research*, 112(A10), A10220. https://doi.org/10.1029/2007JA012368
- Ma, Q., Li, W., Thorne, R. M., Ni, B., Kletzing, C. A., Kurth, W. S., et al. (2015). Modeling inward diffusion and slow decay of energetic electrons in the Farth's outer radiation belt. Geophysical Pagagach Latters, 42(4), 987, 995, https://doi.org/10.1002/2014GU062977
- in the Earth's outer radiation belt. *Geophysical Research Letters*, 42(4), 987–995. https://doi.org/10.1002/2014GL062977

  Ma, Q., Li, W., Yue, C., Thorne, R. M., Bortnik, J., Kletzing, C. A., et al. (2019). Ion heating by electromagnetic ion cyclotron waves and magnetosonic waves in the Earth's inner magnetosphere. *Geophysical Research Letters*, 46(12), 6258–6267. https://doi.org/10.1029/2019GL083513
- Ma, Q., Ni, B., Tao, X., & Thorne, R. M. (2012). Evolution of the plasma sheet electron pitch angle distribution by whistler-mode chorus waves in non-dipole magnetic fields. *Annales de Geophysique*, 30(4), 751–760. https://doi.org/10.5194/angeo-30-751-2012
- Mauk, B. H., Fox, N. J., Kanekal, S. G., Kessel, R. L., Sibeck, D. G., & Ukhorskiy, A. (2013). Science objectives and rationale for the radiation belt storm probes mission. Space Science Reviews, 179(1–4), 3–27. https://doi.org/10.1007/s11214-012-9908-y
- Mitchell, D. G., Lanzerotti, L. J., Kim, C. K., Stokes, M., Ho, G., Cooper, S., et al. (2013). Radiation belt storm probes ion composition experiment (RBSPICE). Space Science Reviews, 179(1–4), 263–308. https://doi.org/10.1007/s11214-013-9965-x
- Miyoshi, Y., Sakaguchi, K., Shiokawa, K., Evans, D., Albert, J., Connors, M., & Jordanova, V. (2008). Precipitation of radiation belt electrons by EMIC waves, observed from ground and space. *Geophysical Research Letters*, 35(23), L23101. https://doi.org/10.1029/2008GL035727
- Morley, S. K., Friedel, R. H. W., Cayton, T. E., & Noveroske, E. (2010). A rapid, global and prolonged electron radiation belt dropout observed with the Global Positioning System constellation. *Geophysical Research Letters*, 37(6), L06102. https://doi.org/10.1029/2010GL042772
- Ni, B., Cao, X., Zou, Z., Zhou, C., Gu, X., Bortnik, J., et al. (2015). Resonant scattering of outer zone relativistic electrons by multiband EMIC waves and resultant electron loss time scales. *Journal of Geophysical Research: Space Physics*, 120(9), 7357–7373. https://doi. org/10.1002/2015JA021466
- Ni, B., Zhang, Y., & Gu, X. (2022). Identification of ring current proton precipitation driven by scattering of electromagnetic ion cyclotron waves. Fundamental Research. https://doi.org/10.1016/j.fmre.2021.12.018
- Shprits, Y., Drozdov, A., Spasojevic, M., Kellerman, A. C., Usanova, M. E., Engebretson, M. J., et al. (2016). Wave-induced loss of ultra-relativistic electrons in the Van Allen radiation belts. *Nature Communications*, 7(1), 12883. https://doi.org/10.1038/ncomms12883
- Tsyganenko, N. A., & Sitnov, M. I. (2005). Modeling the dynamics of the inner magnetosphere during strong geomagnetic storms. *Journal of Geophysical Research*, 110(A3), A03208. https://doi.org/10.1029/2004JA010798
- Tu, W., Cunningham, G. S., Chen, Y., Morley, S. K., Reeves, G. D., Blake, J. B., et al. (2014). Event-specific chorus wave and electron seed population models in DREAM3D using the Van Allen Probes. Geophysical Research Letters, 41(5), 1359–1366. https://doi.org/10.1002/2013GL058819
- Tu, W., Xiang, Z., & Morley, S. K. (2019). Modeling the magnetopause shadowing loss during the June 2015 dropout event. Geophysical Research Letters, 46(16), 9388–9396. https://doi.org/10.1029/2019GL084419
- Turner, D. L., Angelopoulos, V., Morley, S. K., Henderson, M. G., Reeves, G. D., Li, W., et al. (2014). On the cause and extent of outer radiation belt losses during the 30 September 2012 dropout event. *Journal of Geophysical Research: Space Physics*, 119(3), 1530–1540. https://doi.org/10.1002/2013JA019446

LYU ET AL. 7 of 8

- Turner, D. L., Shprits, Y., Hartinger, M., & Angelopoulos, V. (2012). Explaining sudden losses of outer radiation belt electrons during geomagnetic storms. *Nature Physics*, 8(3), 208–212. https://doi.org/10.1038/nphys2185
- Usanova, M. E., Drozdov, A., Orlova, K., Mann, I. R., Shprits, Y., Robertson, M. T., et al. (2014). Effect of EMIC waves on relativistic and ultra-relativistic electron populations: Ground-based and Van Allen Probes observations. *Geophysical Research Letters*, 41(5), 1375–1381. https://doi.org/10.1002/2013GL059024
- Usanova, M. E., Mann, I. R., Kale, Z. C., Rae, I. J., Sydora, R. D., Sandanger, M., et al. (2010). Conjugate ground and multisatellite observations of compression-related EMIC Pc1 waves and associated proton precipitation. *Journal of Geophysical Research*, 115(A7), A07208. https://doi.org/10.1029/2009JA014935
- Xiang, Z., Tu, W., Li, X., Ni, B., Morley, S. K., & Baker, D. N. (2017). Understanding the mechanisms of radiation belt dropouts observed by Van Allen Probes. *Journal of Geophysical Research: Space Physics*, 122(10), 9858–9879. https://doi.org/10.1002/2017JA024487
- Zhang, X.-J., Li, W., Ma, Q., Thorne, R. M., Angelopoulos, V., Bortnik, J., et al. (2016). Direct evidence for EMIC wave scattering of relativistic electrons in space. *Journal of Geophysical Research: Space Physics*, 121(7), 6620–6631. https://doi.org/10.1002/2016JA022521
- Zhao, H., Li, X., Baker, D. N., Claudepierre, S. G., Fennell, J. F., Blake, J. B., et al. (2016). Ring current electron dynamics during geomagnetic storms based on the Van Allen Probes measurements. *Journal of Geophysical Research: Space Physics*, 121(4), 3333–3346. https://doi.org/10.1002/2016JA022358

LYU ET AL. 8 of 8